Diagnostic Nonlinear Analysis of Fischer-Tropsch Synthesis in Stirred-Tank Slurry Reactors

Hyun-Seob Song and Doraiswami Ramkrishna
School of Chemical Engineering, Purdue University, West Lafayette, IN 47907

Sinh Trinh and Harold Wright
Conoco Inc., Ponca City, OK 74602

Multiplicity of steady states was experimentally observed, somewhat sporadically, for Fischer–Tropsch (FT) synthesis in stirred tank slurry reactors in the reactor originally at the wax-producing (normal) steady state suddenly jumping to a high-temperature (methane-producing) steady state for some time and eventually returning to the normal steady state. A diagnostic nonlinear analysis showed a plausible interpretation of this nonlinear behavior under two settings: 1. assuming that the controlled system is stable and motivated by simplicity, as it obviates the inclusion of an energy balance for the cooler, thus reducing the dimension of the problem; 2. examining the more realistic problem by discarding the foregoing assumption, thus having to increase the analysis level. The first approach showed that the Stanton number for heat transfer (St_H) and the Damköhler number (Da) could be two key process parameters accounting for the observed multiplicity characteristics of FT synthesis. The decrease in St_H, attributable to deteriorating performance of the cooler, is the likely cause for the sudden jump of the reactor from the normal to high-temperature steady state. The eventual recovery of the original steady state is, spurred by a decrease in Da, possibly attributable to catalyst deactivation. Depending on the initial conditions and/or startup history from the initial to the target conditions, the multiplicity behaviors of FT synthesis may or may not be observed, which is why the observation of multiplicity is sporadic. The second approach incorporating the cooler's energy balance increases the region of multiplicity over that with the first. Simple proportional control law is applied to the system to examine the effect of the control parameter settings on reactor behavior. Except for this feature, the findings from the two analysis modes are in harmony.

Introduction

Fischer–Tropsch (FT) reactions convert coal-derived synthesis gas, mainly consisting of carbon monoxide and hydrogen, to liquid hydrocarbons as the main products at elevated temperatures and pressure. Bubble-column slurry reactors, among a host of possible reactor configurations for conducting FT reactions, have received special attention due to their good heat-transfer capability enhanced by agitation of the slurry phase, eliminating localized hot spots. This promising temperature-control performance not only reduces the undesirable conversion to methane rather than to liquid hydrocarbon but also makes the progress of catalyst deactivation sluggish. The rational design and operation of bubble-column FT processes requires an accurate understanding of the essential feature of the process, which is, however, hindered by its complex hydrodynamic behaviors (Maretto and Krishna, 1999) and strong nonlinear characteristics (Song et al., 2003). This may be one reason why stirred-tank reactors are often used for fundamental studies of bubble-phase FT processing by several investigators (for example, Satterfield and Huff, 1982; Bukur and Brown, 1987; Bukur et al., 1994). The stirred-tank

Correspondence concerning this article should be addressed to D. Ramkrishna.
Current address of H.-S. Song: LG Chem/Research Park, 104-1 Moonji-dong, Yuseong-gu, Daejeon 305-380, Korea.

reactor configuration can provide a better environment for the analysis of FT processes compared to general bubble-column reactors by achieving uniform distributions of temperature, concentration, and catalyst particles within the reactor.

This study is motivated by some strange nonlinear behaviors experimentally observed in an FT stirred-tank slurry reactor on laboratory scale. Under normal operation, liquid hydrocarbons are constantly produced as the main products, and the product selectivity is in a desirable range. This wax-producing mode continues until the cobalt catalyst requires regeneration due to serious loss of activity. However, occasionally, one encounters multiplicity behaviors that require a detailed understanding of the reaction system. The reaction temperature of the FT process suddenly jumps to a higher value, and accordingly the conversion of the synthesis gas is also increased, undesirably switching the process from FT synthesis mode to methane-producing mode. As a result, the process produces methane instead of liquid hydrocarbons at this high-temperature steady state. Interestingly, the steady state at higher reaction temperature returns to the previous operating steady state after a couple of hours. The conversion of the recovered state is, however, somewhat lower and the selectivity of methane is slightly higher than the one at the starting condition. The objective of this work is to seek a rational explanation for the foregoing phenomenon as well as to elucidate the background of its sporadic character. Further, the analysis will establish the extent to which simplification of reaction kinetics sacrifices its capacity to represent the nonlinear behavior of the reaction system, at least for the stirred reactor. It may not be unreasonable to expect that this investigation could also be used to assess the admissibility of the reaction kinetics to investigate more complex reactor configurations with a view toward improving conversion and selectivity as well as identifying their safety limits of operation.

Shah et al. (1990) have previously made an attempt to address multiplicity behavior of FT reactors. Rather than base such an investigation on the methods of nonlinear analysis, they limited themselves to interpretations based entirely on the heat generation and dissipation curves identified from the data of Bhattacharjee et al. (1986). Thus, ignition and extinction conditions were calculated as functions of process parameters without recourse to rigorous analysis. For a complete elucidation of the multiplicity and stability features of the multidimensional FT reaction system, the thermal analysis of Shah et al. (1990) does not constitute an alternative to the application of rigorous bifurcation theory.

Nonlinear analysis of continuous stirred-tank reactors (CSTR) has been the subject of intensive investigation by engineers and mathematicians, based on the use of catastrophe or singularity theories (Golubitsky and Keyfitz, 1980; Balakotaiah and Luss, 1981, 1983; Farr and Aris, 1986). However, the task at hand is rendered considerably more difficult because of various factors pertinent to FT synthesis: (1) multiphase nature of the system, that is, a solid catalyst phase, a gas phase of reactants and low molecular-weight products, a liquid phase of higher molecular weight products with a potential for a second liquid aqueous phase; (2) a wide-ranging spectrum of gaseous and liquid products; (3) high exothermicity of the reactions; (4) strong interaction between transport and chemical reactions; (5) catalyst deactivation; and numerous others. A consequence of the foregoing complexities, in spite of simplifications, is the high dimensionality of the model system with a large number of variables and parameters, which present one with a cumbersome mathematical problem.

A comprehensive nonlinear analysis has been conducted based on singularity theory to investigate the fundamental reasons for the observed multiplicity behavior. The bifurcation behavior of the system by varying process parameters has been investigated using two approaches. The first is conducted on a simplified model, which assumes that the controlled process is stable and that the dynamics of the controller need not be considered. The second undertakes the burden of the full problem with a proportional controller for the coolant flow rate. In view of the potential for deterioration in the performance of the cooler and activity of the catalyst, with the progress of reaction, special focus was placed on the effects of the Stanton number for heat transfer (St_H) and the Damköhler number (Da) on the bifurcation behaviors of the process. The sequel to the analyses has shown that deterioration of heat removal performance and catalyst deactivation with time could reasonably account for the observed nonlinear characteristics of FT synthesis reactors. The former effects are reflected into St_H and the latter into Da in the derived dimensionless model equations, as will be established subsequently. The decrease in St_H, a consequence of the diminishing heat-transfer coefficient between the coolant and the reaction medium, is shown to cause a sudden jump from the normal steady state (or wax-producing model) to the high-temperature steady state (or methane-producing mode). Thereafter, decrease in Da, attributable to progressing catalyst deactivation, presents a possible explanation for the restoration of the normal operating steady state, albeit with a conversion and selectivity lower than before. We also establish that, depending on the initial condition and startup history, the steady-state transition between the wax- and the methane-producing mode may or may not happen in FT synthesis reactions. Furthermore, we show how this nonlinear behavior can be sporadic through a global bifurcation diagram in the St_H and Da space. We stress that the accomplishment of this article is a testimonial to the effectiveness of nonlinear analysis in diagnosing the origin of a practical industrial problem.

Model Formulation

In most published models the FT process is generally represented by a combination of the main FT synthesis (that is, the production of hydrocarbons) and water–gas shift (WGS) reactions, of which the latter is considered to be inactive for cobalt-based catalysts being dealt with here. The net reaction conducted under cobalt-based catalysts can be grossly represented as follows

$$(-\nu_1)\mathrm{H}_2 + (-\nu_2)\mathrm{CO} \rightarrow \nu_3 \mathrm{C}_n\mathrm{H}_m + \nu_4 \mathrm{H}_2\mathrm{O} \qquad (1)$$

The stoichiometric coefficients and the average number of carbon (n) and hydrogen (m) of the obtained hydrocarbon products can be expressed in terms of the chain-growth prob-

ability factor (α) and the paraffin fraction in the reaction products (β) as shown below (Stern et al., 1985)

$$\nu_1 = -\left[2 + (1-\alpha)^2 + \beta\alpha(1-\alpha)\right] \quad (2)$$

$$\nu_2 = -1 \quad (3)$$

$$\nu_3 = 1-\alpha \quad (4)$$

$$\nu_4 = -\nu_2 \quad (5)$$

and

$$n = (1-\alpha)^{-1} \quad (6)$$

$$m = 2\left[(1-\alpha)^{-1} + (1-\alpha) + \beta\alpha\right] \quad (7)$$

Hereafter, the subscripts 1, 2, 3, and 4 denote hydrogen, carbon monoxide, hydrocarbon, and water, respectively. Among other available kinetic models of FT synthesis in the literature, the following equation is selected as the most appropriate form for cobalt catalysts (Withers et al., 1990; Kirillov et al., 1999)

$$R = \left(\frac{\nu_2}{\nu_1+\nu_2}\right)\frac{kC_1^2C_2}{C_1^2C_2 + KC_4} \quad (8)$$

Instead of considering all the complex reaction mechanisms involved in FT synthesis, the simple Anderson–Schultz–Flory (ASF) equation is adopted here to describe the product selectivity. The mole fractions of hydrocarbons with the number of carbons equal to i are given as a function of the chain-growth probability factor (or also called ASF factor), α

$$x_i = (1-\alpha)\alpha^{i-1} \quad (9)$$

The determination of the parameter α is of great importance in that it would govern the product distribution as well as affect the stoichiometric coefficients of the FT reaction together with the parameter β just given. While the value of β has been fixed as 0.85 (that is, 85% paraffin in the hydrocarbon products) throughout the calculation in this study, we have tried to consider the functional dependence of α on the reaction conditions as much as possible. For example, the temperature dependence of α should essentially be incorporated into the model in order to account for the product selectivity changes at different states, that is, the FT process mainly forms liquid hydrocarbons under the usual operating conditions, which would, however, be replaced by methane gas at the high-temperature steady state as described in the beginning of this article.

Unfortunately, aside from a concentration dependence, a generally acceptable explicit correlation of α with reaction conditions is not available in the literature. (Lox and Froment (1993a,b) proposed α as a function of temperature and reaction mixture composition for an iron catalyst, but that correlation is not used here because it is shown to be inappropriate for our system based on cobalt catalysts.) In an experiment over an alumina-supported cobalt catalyst promoted with zirconium, Yermakova and Anikeev (2000) suggested, after testing several different equations, the following empirical functional relation between α and the compositions of H_2 and CO

$$\alpha = A\frac{y_2}{y_1+y_2} + B \quad (10)$$

where y indicates the mole fraction of the gas-phase component. The model parameters A and B are assigned as constant values (that is, $A = 0.2332 \pm 0.0740$ and $B = 0.6330 \pm 0.0420$) because all the variables other than compositions have been fixed in their experimental work. This equation can be applied to the limited case where only compositions are changing. To extend the usage of Yermakova and Anikeev's model and, more importantly, to make our model capable of explaining the significant changes of the product composition between the two different observed steady states, Eq. 10 is slightly modified by adding temperature dependence as a simple linear function as follows

$$\alpha = \left(A\frac{y_2}{y_1+y_2} + B\right)\left[1 - 0.0039(T-533)\right] \quad (11)$$

Equation 11 is immediately reduced to Eq. 10 by setting $T = 533$ K, the temperature for which Eq. 10 is derived. It should be noted that this equation is only applicable to the range of the operating conditions rendering $0 \le \alpha \le 1$. The slope of temperature dependence has been fitted to various experimental data summarized in Figure 13 of a recent article by Van Der Laan and Beenackers (1999).

The principal assumptions in the formulation of this model are summarized as follows:

(1) The mass-transfer resistance between liquid phase and solid catalysts is neglected, so that we need consider only two phases of gas and slurry in mass balances.

(2) The gas and slurry phases are well mixed and the species concentrations in each phase are constant.

(3) The catalyst particles are uniformly distributed in the reactor.

(4) The gas phase obeys the ideal gas law.

(5) The heat-transfer resistance between the two phases is neglected so that the temperature is constant throughout the reactor.

(6) The coolant is assumed to be well-mixed in the cooler so that its temperature can be regarded as constant.

(7) There is no input or output of slurry associated with the reactor.

(8) The process parameters involved in modeling such as gas holdup, heat capacities, and densities, are constant.

Under the foregoing assumptions, the steady-state equations are written in dimensionless form

$$\phi_{Gj,0} - q_G\phi_{Gj} - St_j(\phi_{Gj} - \phi_{Lj}) = 0 \quad (j = 1,\ldots,ns) \quad (12)$$

$$St_j(\phi_{Gj} - \phi_{Lj}) + \nu_j Da\psi = 0 \quad (j-1,\ldots,ns) \quad (13)$$

$$\left(\sum_{j=1}^{ns}\phi_{Gj,0} - q_G\tilde{P}/\theta\right) - \sum_{j=1}^{ns} St_j(\phi_{Gj} - \phi_{Lj}) = 0 \quad (14)$$

$$(\Omega_{G,0}\theta_{G,0} - q_G\Omega_G\theta) - St_H(\theta - \theta_C) + Da\psi Be_R = 0 \quad (15)$$

where ns indicates the number of species that is 4 in our model, ϕ, θ, q, $\tilde{P}$, St, St_H, Be_R, Da, ψ, and γ indicate concentration, temperature, flow rate, pressure, Stanton numbers for mass and heat transfer, heat of reaction, Damköhler number, and activation energy, respectively, and the physical implication of the other dimensionless parameters can be readily inferred from their definitions given below. The subscripts G, L, 0, j denote gas phase, liquid (or slurry) phase, inlet condition, and species j, respectively

$$\phi_{Gj,0} = \frac{C_{Gj,0}}{C_{G1,0}}, \qquad \phi_{Gj} = \frac{C_{Gj}}{C_{G1,0}}, \qquad \phi_{Lj} = \frac{C_{Lj}}{C_{G1,0}}$$

$$q_G = \frac{Q_G}{Q_{G,0}}, \qquad \theta_{G,0} = \frac{T_{G,0}}{T_{C,0}}, \qquad \theta = \frac{T}{T_{C,0}}$$

$$\theta_C = \frac{T_C}{T_{C,0}}, \qquad \tilde{P} = \frac{P}{C_{G1,0}RT_{C,0}}, \qquad \Omega_{G,0} = \frac{\rho_{G,0}C_{pG,0}}{\rho_L C_{pL}}$$

$$\Omega_G = \frac{\rho_G C_{pG}}{\rho_L C_{pL}}, \qquad St_j = \frac{(k_L a)_j}{He_j Q_{G,0}/V}$$

$$St_H = \frac{h_C a_C}{\rho_L C_{pL} Q_{G,0}/V}, \qquad Be_R = \frac{(-\Delta H_R)C_{G1,0}}{\rho_L C_{pL} T_{C,0}}$$

$$Da = \frac{w(1-\epsilon_G)a_{cat}k(T_{C,0})/He_1}{Q_{G,0}/V}$$

$$\psi = \exp\left[-\gamma\left(\frac{1}{\theta}-1\right)\right]\frac{\phi_{L,1}^2\phi_{L,2}}{\phi_{L,1}\phi_{L,2}+\tilde{K}\phi_{L,4}}$$

$$\gamma = \frac{E}{RT_{C,0}}, \qquad \tilde{K} = K\frac{He_1He_2}{C_{G1,0}He_4} \tag{16}$$

The nominal values for the preceding dimensionless parameters are given in Table 1. Equations 12 to 15 are the mass balance of species i in the gas phase, the overall mass balance of the gas phase, the mass balance of species i in the slurry phase, and energy balance, respectively.

Table 1. Nominal Values for the Model Parameters

	Dimensionless Values
Feed conditions	$\phi_{G1,0} = 1$, $\phi_{G2,0} = 0.5$, $\phi_{G3,0} = 0$, $\phi_{G4,0} = 0$, $\theta_{G,0} = 0.6928$
Stanton nos. for heat and mass transfer	$St_H = 0.38$, $St_1 = 5.3423$, $St_2 = 7.5196$, $St_3 = 3.8956$, $St_4 = 37.761$
Reaction parameters	$Da = 0.01225$, $Be_R = 0.3021$, $\gamma = 27.657$, $\tilde{K} = 0.12067$
Pressure and temp.	$\tilde{P} = 1.0392$, $\theta_{\mathrm{SET}} = 1.1772$
Others	$\Omega_{G,0} = 0.0097$, $\Omega_G = 0.0057$, $\Omega_{C,0} = \Omega_C = 0.000934$, $\delta = 20$

Local Multiplicity Behavior

Examination of possible causes

A typical S-shaped temperature profile is obtained by solving the model equations given by Eqs. 12 to 15 based on the parameter values of Table 1 (Figure 1). The dotted and the solid lines in Figure 1 indicate the unstable and the stable steady-state solutions, respectively. The nominal operating temperature of the FT reactor is around 1.1772, as marked by solid circle in Figure 1. This figure shows that careful operations are necessary to maintain the process at this unstable intermediate steady state. The process may go astray from this unstable state to upper or lower stable steady state when small disturbances are introduced unless appropriate control actions are taken. At this stage, we present two modes of analysis in this article. We at first assume that the process can be stabilized by feedback controllers throughout the operation, that is, no unstable steady states exist in our system in the closed-loop context. This premise is justified in a later section investigating the effects of control-parameter settings on the stability and multiplicity behavior of the same process. Indeed improper tuning of control parameters might be responsible to some extent for the runaway behavior, especially when the process characteristics are significantly changed during operation. However, in order to examine this issue, we extend the analysis to include an additional energy balance around the cooler, thus increasing by one the already sizable set of equations. The simpler approach considered at first, however, has the advantage of enlightening us with the proper range of process parameters without having to be burdened with the full set of equations.

Another problem in the operation of our FT process found from Figure 1 may be the ignition and/or extinction risks around the two turning points due to the hysteresis characteristics of the process. This issue has been theoretically treated by Shah et al. (1990) based on the experimental observation by Bhattacharjee et al. (1986), where the critical conditions for ignition and extinction are provided in terms of the various process parameters, such as CO feed concentration, gas space velocity, and activation energy. They warned that it is essential to avoid the ignition. Once the ignition

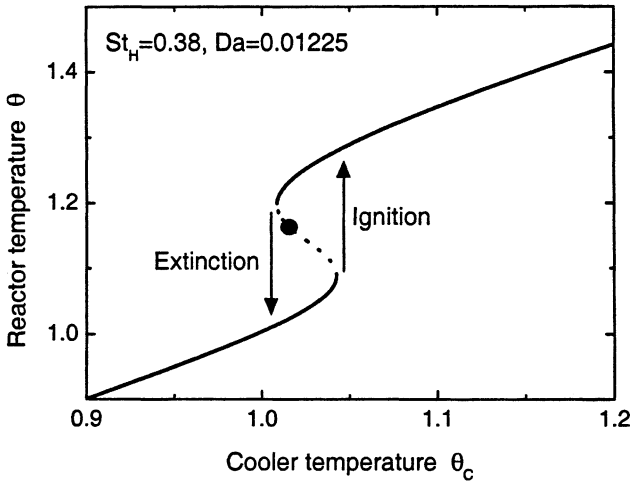

Figure 1. Sigmoidal temperature curve obtained with parameters given in Table 1.

occurs, the normal FT synthesis reaction would be switched to the methane-forming mode, seemingly never to return. This is because the catalyst could suffer serious deactivation on exposure to the high temperature resulting from the ignition. However, the evidence, sporadic as it may be, is contrary to the scenario just suggested. First of all, as identified in Figure 1, the possibility of ignition is very low as the nominal operating condition of the FT process is far away from the ignition temperature. In fact, this situation is more conducive to extinction than ignition, one that has never arisen in our reactor facilities. Furthermore, the subsequent return after some hours to the properly steady state (even granting the lower selective conversion) is in sharp contrast to the observation by Bhattacharjee et al. (1986). The foregoing arguments provide strong evidence against ignition being the underlying mechanism for the steady-state transition of our system. Also, the actual reactor temperature after the runaway, which had been monitored during operation, was significantly lower than the one to be realized by the ignition predicted by our model.

From the arguments presented earlier, we have ruled out two possibilities in the interpretation of the multiplicity behavior displayed by our FT reactor. The first, which discounts instability arising from poor tuning of control parameters, is somewhat arbitrary for the present, but one that is justified in a later selection, which discusses the more detailed analysis incorporating the cooler and controller dynamics. The second rules out ignition in accord with the arguments presented in the preceding paragraph. This, however, should imply that the normal steady state should prevail, as the reactor parameters would seem to be safely off the limits of a steady-state switch. The conclusion just made is on the presumption that all process parameters must remain invariant with time. Naturally, an explanation for the disturbance of status quo must take root in the dynamic variation of some key parameters with time, perhaps on a much slower time

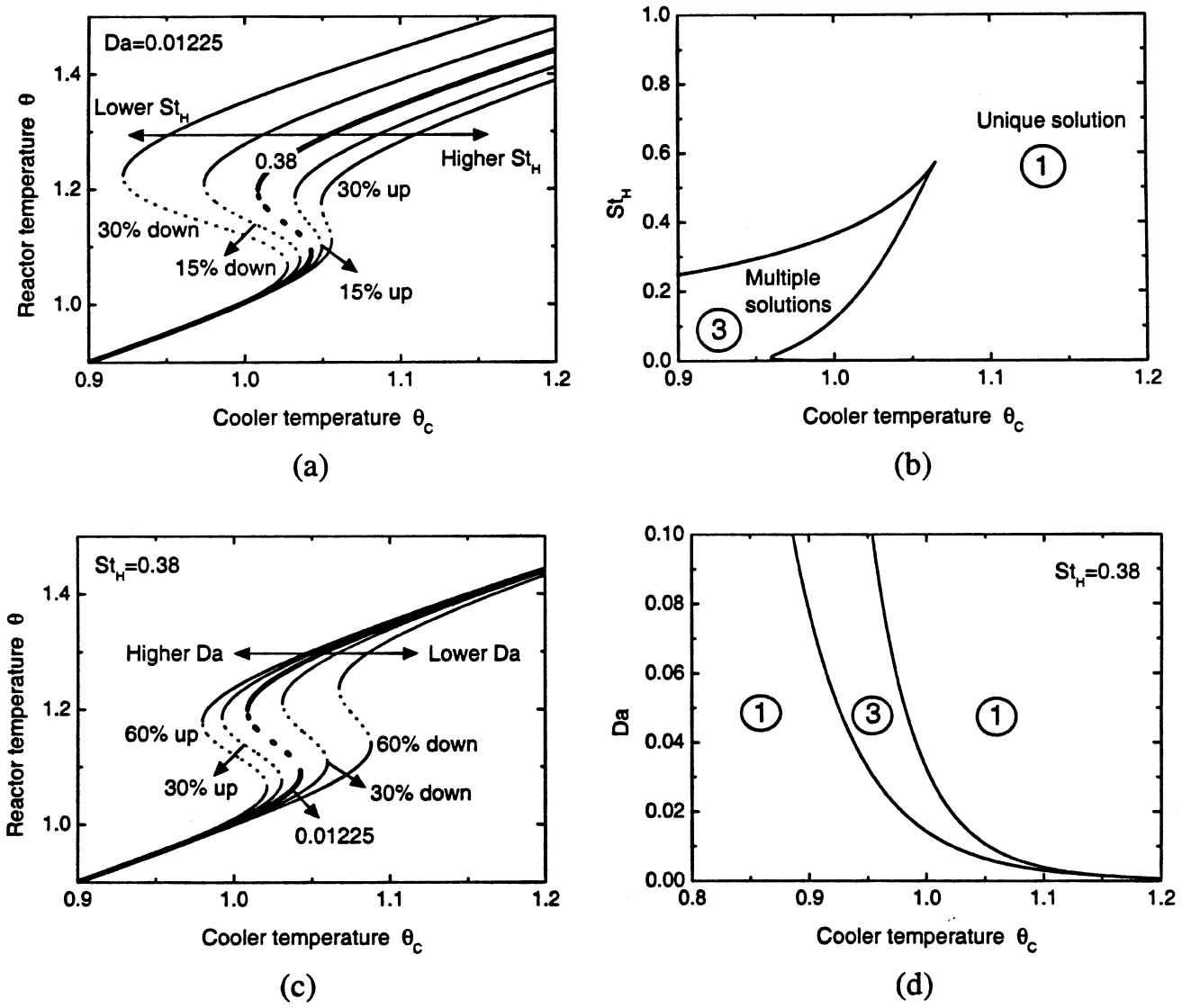

Figure 2. Effects of the variation St_H [(a) and (b)] and Da [(c) and (d)] on the shape of temperature curves on the $(\theta\text{-}\theta_c)$ plane and the multiplicity map on the $(St_H\text{-}\theta_c)$ plane.

scale. The steady-state shift must occur as a consequence of a dynamic change in one or more process parameters. More precisely, we envisage, some parameters varying with time in a way such that the process characteristics are altered significantly. From this consideration, two key process parameters that are believed to be responsible for our problem are suggested here: the heat-transfer coefficient between the cooler and the reactor and activity of the catalyst.

The overall heat-transfer coefficient, h_c, or, in other words, the heat-removal performance of the cooler, would decrease with time due to fouling of the surface and/or increasing viscosity of the reaction medium, or possibly other reasons. The heat-transfer coefficient is contained in St_H, which is proportional to the ratio of the convective heat transfer to the thermal capacity of fluid as defined in Eq. 16. We can directly regard St_H as the measure of the heat-removal capability of the cooler because all the parameters except the heat-transfer coefficient are assumed to be constant in the definition of St_H. Thus, St_H is no more than the dimensionless version of the heat-transfer coefficient in this article. On the other hand, the catalyst activity, a_{cat}, appears in Da as defined in Eq. 16. At the outset, the activity parameter would be assumed to be unity, that is, no catalyst deactivation. However, it would gradually diminish as the concentration of active sites in the catalyst decreases with the progress of the reaction. The activity of cobalt catalysts in FT slurry reactors can be decreased by the high temperature, the accumulation of the longer hydrocarbons surrounding the catalysts, or any other poisoning factors (Liu et al., 1997; Gormley et al., 1997). The effects of water on the FT cobalt catalysts were varied, probably depending on the support materials, promoters, cobalt precursors, and preparation methods (Hilmen et al., 1999). Da indicates the ratio of reaction rate to the convective transport rate, but we can simply interpret Da as the measure of the catalyst's activity here. Incorporating these transient parameters into our model is not difficult, as one expects that the time scales for both the decreasing St_H and the decreasing Da are quite large compared to the process characteristic times for reaction, convection, and diffusion; thus, it can be assumed that the process immediately arrives at steady state at every instant during the period that these two parameters are varying. This assumption validates the steady-state model equations, Eqs. 12 to 15, even during the transient period of a deteriorating performance of the cooler and catalyst activity.

A scenario for experimental observations

In order to connect the variation of these two parameters with the observed multiplicity behaviors, local sensitivity tests have been conducted around the nominal operating conditions. First, effects of St_H are shown in Figure 2a, where the thicker line indicates the standard initial operating curve. These trends of Figure 2a are readily interpreted. For example, high St_H means that we have a good cooler with a high heat-transfer coefficient or with a large heat-transfer area. The shift of the temperature profile to the right with higher St_H may be interpreted as the increase of the cooler temperature for keeping the reactor temperature at the target value. A small temperature difference between the reactor and the cooler would be sufficient to control the reaction temperature for high St_H. The reverse explanation holds for small St_H. Thus, it is seen that the increase (decrease) of St_H has a favorable (unfavorable) effect in regard to multiplicity. High St_H, that is, good heat-removal performance of the cooler, suppresses the possibility of multiple steady state by diminishing the nonlinear heat-generation effects and vice versa (see also Figure 2b).

The effects of Da are quite different from those of St_H. As shown in Figure 2c, increase (or decrease) in Da requires a lower (or higher) cooler temperature for keeping the desired steady state, which is exactly the opposite effect of St_H. This behavior obviously arises from Da multiplying the heat of reaction term. The decrease of Da has little effect on the shape of the temperature profile, at least around the nominal condition, although the S-shape will eventually disappear when Da approaches zero (see Figure 2d).

Based on the effects of St_H and Da on the process behavior, we suggest a possible scenario for the observed multiplicity phenomenon. We expect in reality that both of these two parameters would decrease with time as the reaction proceeds due to reasons that were deliberated earlier. The time scale of this drifting behavior would require more extended vigilance on the reactor performance. Consequently, we have restricted our goal here to elucidating how the experimental observations are related to the gradual decrease of St_H and Da.

We suppose for the present that the drift rate of (decreasing) St_H is initially dominant compared to that of Da. At the extreme, we can assume that only St_H is decreasing while Da remains constant, that is, the heat-transfer coefficient gets smaller with time without the catalyst deactivation. From the preceding deliberations, as St_H becomes smaller, the cooler temperature should adaptively diminish to maintain the operating steady state (Figure 3a). However, there is a limit below which the coolant temperature cannot be lowered. This lower limit is in the *inlet* coolant temperature, which would be realized only when the coolant flow rate approaches infinity. Since all the dimensionless temperatures have been defined as the ratio of this inlet coolant temperature as shown in Eq. 16, the lower limit of the dimensionless cooler temperature is unity. Thus, the feasible domain corresponds to the region where the cooler temperature is above unity. If the reactor temperature belongs to the infeasible domain (that is, the region of $\theta_c < 1$), it would not be achieved as a steady state due to the lack of further cooling capability. With initial St_H, the process would stay at the target temperature (the profile A in Figure 3a); however, it would be impossible to maintain this temperature anymore when St_H becomes quite smaller (such as the profile C). The critical situation is when the target temperature is exactly at the limiting value of the manipulated variable (the profile B). Under this situation, the slightest disturbance introduced into the system would temporarily cause the shift of steady state either toward the upper or the lower one. Of these two possible shifts, the transition to the lower steady state is preventable, since its pathway lies in the feasible region. However, there is no way to bring down the increasing temperature along the infeasible runaway route to the upper steady state. This is a plausible explanation of why and how the reaction temperature suddenly jumps to the higher one during operation. The reactor temperature becomes progressively higher as St_H continues its decrease fur-

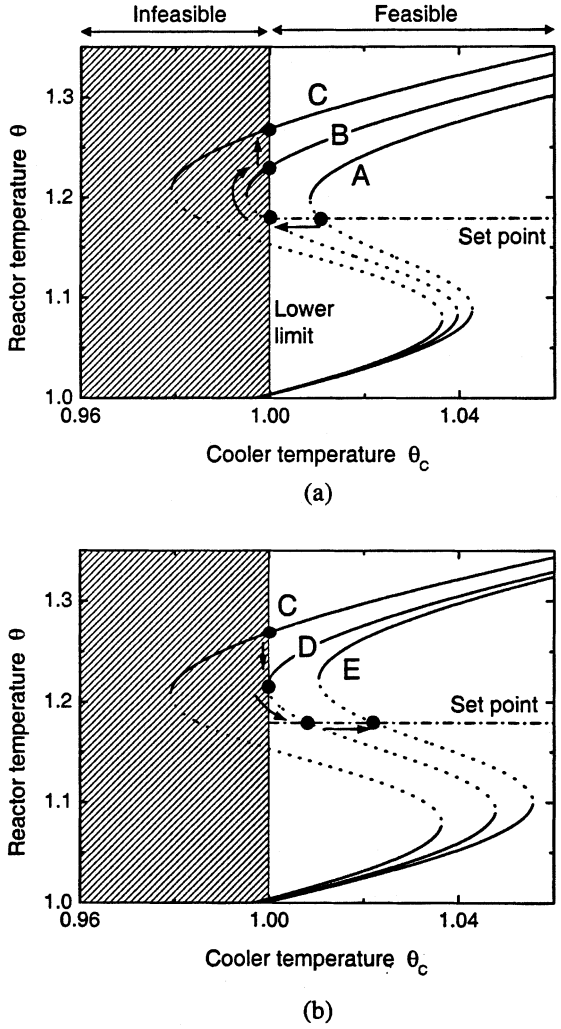

Figure 3. (a) Steady-state jumping from the normal wax-producing mode to the methane-formind mode with the decrease of St_H; (b) eventual recovery of the previous steady state with the decrease of Da.

ther. At the high reaction temperature, the main product of FT reactors will switch from the liquid hydrocarbons to methane gas. As pointed out earlier, this phenomenon should be distinguished from a typical ignition phenomenon. For the latter to occur, the process should be in operation at the lower steady-state branch of the sigmoidal temperature curve near its turning point to the *right*. At these low reaction temperature conditions, however, the expected conversion is considerably below that which is observed at the beginning. It might be interesting to see whether or not a Hopf bifurcation forms as St_H decreases in Figures 2a and 3a. In order to determine this, we investigated the existence of a simple pair of purely imaginary eigenvalues of the Jacobian matrix at every point along the temperature curves throughout the calculation, but they were never found. The definition of the Jacobian matrix will be given later.

Next, we address the eventual return of the upper steady state to the normal operating steady state. Once the reactor temperature is boosted up to a higher value, the rate of catalyst deactivation would be enhanced by sintering or other factors. The consequent decrease of Da by the catalyst deactivation would push back the temperature profile to the feasible region (such as from the profile C toward the profile E) as shown in Figure 3b. It should be noted that the critical condition for the desirable intermediate state to be restored is different from that of the initial jump. The previous steady state is not recovered until the *left* turning point of the sigmoidal temperature curve passes the limiting line of the cooler temperature (the profile D). This is because the returning pathway to the normal condition is rendered inaccessible by the infeasible region before the left turning point enters the feasible region. The main products at the restored normal condition again become the heavy hydrocarbons rather than methane gas, although the conversion is decreased somewhat by deactivation of the catalyst. The recovery of the normal wax-producing mode from methane production is clear evidence that the runaway behavior observed in our system is *not* due to ignition. If the runaway were caused by the ignition, the reactor temperature at the new steady state would be high enough to seriously deactivate the catalyst, making the recovery to the wax-producing mode virtually impossible.

Global Multiplicity Features

From the local sensitivity analysis given earlier, we could provide a reasonable answer to the question of how and why the normal FT synthesis mode is suddenly switched to the higher temperature state with the production of mainly methane, eventually returning again to the original operating state with some loss of conversion. However, it remains to elucidate the critical values of St_H and Da at which the foregoing transitions occur. Moreover, we also need to throw some light on the sporadic nature of the transitions. Toward this end, we seek to analyze the global multiplicity features of the system. These questions will be clear from the global multiplicity portrait over the parameter space of St_H and Da, which will be constructed using advanced nonlinear analysis tools in the following sections.

Liapunov-Schmidt (L-S) Reduction and Singularity Theory

The model equations of our system, Eqs. 12 through 15, can be rewritten in the following general form

$$\boldsymbol{f}(\boldsymbol{x},\boldsymbol{p}) = \boldsymbol{0} \tag{17}$$

where the n-dimensional vector $\boldsymbol{x}$ denotes the 10 state variables, that is, 8 species concentrations in the gas and slurry phases, overall gas velocity, and reactor temperature, and the m-dimensional vector $\boldsymbol{p}$ indicates the bifurcation and process parameters, that is, θ_c, St_H, and Da. The mapping $\boldsymbol{f}: R^n \times R^m \rightarrow R^n$ is assumed to be infinitely differentiable with respect to $\boldsymbol{x}$ and $\boldsymbol{p}$. Comprehensive nonlinear analysis of a set of highly nonlinear equations like Eq. 17 becomes cumbersome when the dimensionality of system equations and the number of parameters are large. The difficulties of doing this task could be substantially relieved if we could reduce the number of model equations into one using the analytic relations between the variables. Explicit representation of one

variable in terms of the other ones is, however, impossible for the system at hand, because of the complex functional dependences of the parameters; more specifically, the stoichiometric coefficients of Eqs. 2 to 5 depend on the chain-growth probability factor α, which is in turn a function of the reactor temperature and the species composition, as suggested in Eq. 11.

The Liapunov-Schmidt (L-S) reduction technique can be applied for this case when global reduction based on explicit functional relations of variables is not possible. The L-S technique reduces the system equations and variables locally into a smaller set around a singular point. Especially, for the case that the Jacobian matrix has a rank-deficiency one, a single scalar equation is obtained. The reduced equations and the reduced variables are called the branching equations and the intrinsic state variables, respectively. The L-S reduction technique does not simplify the finding of the solutions of the equations, but significantly simplifies the examination of the local multiplicity features of the system by readily providing expressions for high-order derivatives of the reduced single equation as a convenient form to apply. In some sense, the L-S decomposition is concentrating the nonlinearity into the reduced equations and removing the linearity. For details of the L-S reduction procedure, see Golubitsky and Schaeffer (1979, 1985), Balakotaiah and Luss (1984), and Balakotaiah et al. (1985).

The determination of the number of branching equations is difficult in the present case because of the analytically complex structure of the Jacobian matrix. Using the symbolic manipulators, some off-diagonal terms of the Jacobian matrix obtained are found to be nonzero due to the nonlinear interaction between the variables. Consequently, the extent of the reduction could be checked only numerically by evaluating the rank of the Jacobian matrix at the singular point throughout the calculations. Fortunately, as the rank could be determined to be $(n-1)$ at least, our system equations could be reduced to a single equation using the L-S decomposition procedure. The resulting form of the reduced equation is expressed as

$$g(y,\theta_c,St_H,Da)=0 \tag{18}$$

Any component of $\boldsymbol{x}$ can be selected as the intrinsic state variable y, but the reactor temperature θ was chosen, as it seemed the most appropriate in our context. Analysis of the branching equation of Eq. 18 is amenable to elementary catastrophe theory or to the more general singularity theory (Gilmore, 1981; Golubitsky and Schaeffer, 1985). The essence of the singularity theory lies in the same qualitative local behaviors of the branching equation and the original equations around the singular point, which is called *contact equivalence*. All the possible bifurcation features of the original system can thus be obtained through the nonlinear analysis of the single branching equation instead of examining the whole set of the model equations. The power of singularity theory lies in its capacity to unravel diverse features of steady-state multiplicity in nonlinear systems. Particularly noteworthy among these is the determination of the most singular point, that is, that of maximum multiplicity. However, our quest in this article is limited only to tuning points and hysteresis. Application of the singularity theory (in conjunction with the method of continuation) makes it possible to investigate the foregoing singular points in the parameter space of St_H and Da. The locus of hysteresis points plotted in the St_H–Da plane will separate the region of multiplicity from that of unique steady states. Clearly, this is a central issue to the current investigation.

Critical boundaries and overall multiplicity portrait

Thus, from the foregoing discussion we can identify in the St_H–Da plane three important critical conditions of interest to our system: hysteresis locus, control-limit boundary, and disjoint loci. Control-limit boundary and disjoint loci predict the critical situations of the steady-state transitions. The former provides information as to when the process will jump from the nominal to the high-temperature steady state, while the latter determine the point of eventual return to the previous steady state. These two boundaries are significant to our interpretation of the experimental observations. In view of our specific interest in diagnosing the underlying cause of the FT reactor behavior outlined in the Introduction, we shall sacrifice a more general treatment of the reactor equations within the scope of singularity theory. There of course remains the question of whether or not other forms of singularities may be important for our diagnostic quest. In this regard, our investigations including additional parameters led to no discoveries of other forms of singularities. However, it is not inconceivable that there may exist some parameter ranges, which may allow alternative nonlinear behavior. This is an uncertainty with which one must always contend.

Calculation of the hysteresis points requires the vanishing of up to second-order derivatives of second-order derivatives of the branching equation with respect to the intrinsic state variable. The corresponding defining and nondegeneracy conditions for hysteresis are

$$g=g_y=g_{yy}=0 \qquad \text{and} \qquad g_{yyy}\neq 0 \tag{19}$$

The parameter θ_c is chosen as a bifurcation parameter, while St_H and Da are treated as process parameters, all of which are to be determined together with the intrinsic state variable y (that is, θ here) by solving Eq. 19. The single degree of freedom implicitly in Eq. 19 enables the construction of the required hysteresis locus in the St_H–Da plane.

It should be noted that the branching equation g in Eq. 19 is not given as an *explicit* form in our system, but only in an *implicit* sense. In what follows, the reader unfamiliar with the L-S reduction procedure can skip the treatment following immediately (as it is only concerned with the technical details of implementing Eq. 19) and proceed directly to the part following Eq. 27.

The full set of original model equations (Eq. 17) should be handled to implement the conditions in Eq. 19. Given St_H and Da, the first two equations of Eq. 19, that is, $g=g_y=0$, can be alternatively written as the following set, which has been called a *branching system* or the *Munich system* (Seydel, 1994)

$$\boldsymbol{f}(\boldsymbol{x},\theta_c)=\boldsymbol{0} \tag{20}$$

$$\boldsymbol{L}\boldsymbol{h}=\boldsymbol{0} \tag{21}$$

$$h_k-1=0 \tag{22}$$

Equation 21, in view of Eq. 22, is equivalent to the Jacobian matrix $\boldsymbol{L}^2$ (the Jacobian matrix, $\boldsymbol{L} \equiv [\partial f_i/\partial x_j]$ $(I = 1, 2, \ldots, n;$ $j = 1, 2, \ldots, n)$ being singular. That is, if the linearized system Eq. 21 has a nontrivial solution $\boldsymbol{h}_0 \neq \boldsymbol{0}$, then we will have a rank-deficient Jacobian matrix. Equation 22 is necessary to choose one solution vector among the infinite candidates for $\boldsymbol{h}_0$, where the subscript k therein can be any integer value between 1 and n ($= 10$ here). The equations are closed since we have 21 unknowns of $\boldsymbol{x}$, $\boldsymbol{h}$, θ_c for 21 equations with St_H and Da fixed.

The second- and third-order derivatives of the branching equation in Eq. 19 can be readily calculated by the formulas derived by the L-S procedure (Golubitsky and Schaeffer, 1985)

$$g_{yy} = \langle \boldsymbol{v}_0^*, d^2\boldsymbol{f}(\boldsymbol{v}_0, \boldsymbol{v}_0) \rangle \tag{23}$$

$$g_{yyy} = \langle \boldsymbol{v}_0^*, d^3\boldsymbol{f}(\boldsymbol{v}_0, \boldsymbol{v}_0, \boldsymbol{v}_0) - 3d^2\boldsymbol{f}\big(\boldsymbol{v}_0, \boldsymbol{L}^{-1}\boldsymbol{E}d^2\boldsymbol{f}(\boldsymbol{v}_0, \boldsymbol{v}_0)\big) \rangle \tag{24}$$

where the symbol $\langle\ \rangle$ indicates the inner product and $\boldsymbol{E}$ is the projection operator onto the range of $\boldsymbol{L}$, $\boldsymbol{v}_0^*$ and $\boldsymbol{v}_0$ are n-dimensional vectors satisfying

$$\boldsymbol{L}\boldsymbol{v}_0 = \boldsymbol{0} \tag{25}$$

$$\boldsymbol{L}^*\boldsymbol{v}_0^* = \boldsymbol{0} \tag{26}$$

where $\boldsymbol{L}^*$ is the adjoint matrix of $\boldsymbol{L}$. The kth differential of the vector function $\boldsymbol{f}$ at $(\boldsymbol{x}, \boldsymbol{p})$ can be represented in terms of the kth partial derivatives of $\boldsymbol{f}$, for example, if $k = 3$, then

$$(d^3\boldsymbol{f})_{(\boldsymbol{x},\boldsymbol{p})}(\boldsymbol{u}, \boldsymbol{v}, \boldsymbol{w}) = \sum_{i,j,k=1}^{n} \frac{\partial^3 \boldsymbol{f}}{\partial x_i \partial x_j \partial x_k}(\boldsymbol{x}, \boldsymbol{p}) u_i v_j w_k \tag{27}$$

Now, we are ready to calculate overall hysteresis locus over the global parameter space of St_H and Da. The detailed calculation procedure is shown in Figure 4. As a starting value, with a chosen St_H, we find the corresponding Da (and $\boldsymbol{x}$, $\boldsymbol{h}$, and θ_c) satisfying the hysteresis conditions of Eq. 19 using Eqs. 20–23. Then, the next solution set of (St_H and Da) is continued using the prediction and correction procedures based on the continuation method (Seydel, 1994) at the outer loop, while the calculation of the singular point is being done in the inner loop. The possibility of the third-order derivative g_{yyy} to be zero has been checked at each hysteresis point during this calculation procedure, but never found throughout the calculations.

Next, we calculate the criterion for the process to jump to a high-temperature steady state. This abnormal runaway behavior will occur when the process arrives at some critical situation, when the reactor temperature cannot be maintained at the setpoint any more (see Figure 3a). Here we call the locus of such critical points the *control-limit boundary* (B in Figure 3a), the definition of which is given by

$$g = 0, \qquad \theta_c = 1, \qquad \text{and} \qquad \theta = 1.1772 \tag{28}$$

The first condition of Eq. 28 is for the steady state, the second signifies that the control action is bound by its lowest value, and the third anchors the reactor temperature at the set point. The numerical procedure of obtaining the control-limit boundary does not clearly include the calculation of singular points. We only have to track the sets of St_H and Da by solving the steady-state equations, excluding the energy equation, because the reactor temperature is fixed at the target value of $\theta = 1.1772$.

The control-limit locus has been drawn together with the hysteresis locus in Figure 5a, where the parameter space is divided into three different regimes. Regime (I) is distinguished from regimes (II) and (III) by the temperature curve being S-shaped there. Multiplicity behavior can be observed only when the process belongs to regime (II) or (III). Further, regime (III) is distinguished from regimes (I) and (II) in that it does not allow the reactor temperature to be maintained at the set value. If the process crosses the control boundary from (II) to (III), as by the increase of Da and/or the decrease of St_H, it will happen that the normal steady state jumps to a high-temperature steady state. The control-limit boundary of Figure 5a thus shows, within the context presented by our model, when the process can jump from the normal wax-producing mode to the methane-forming mode.

The other critical situation of interest is the potential return of our system to the previous steady state. As shown earlier, when the left turning point of the temperature profile goes beyond the lower limit of the cooler temperature from the infeasible to the feasible region, the initial steady state is finally restored. These conditions can be expressed as follows

$$g = g_y = 0 \qquad \text{and} \qquad \theta_c = 1 \tag{29}$$

Of course, the foregoing conditions do not discriminate between the left and right turning points. Although, our specific

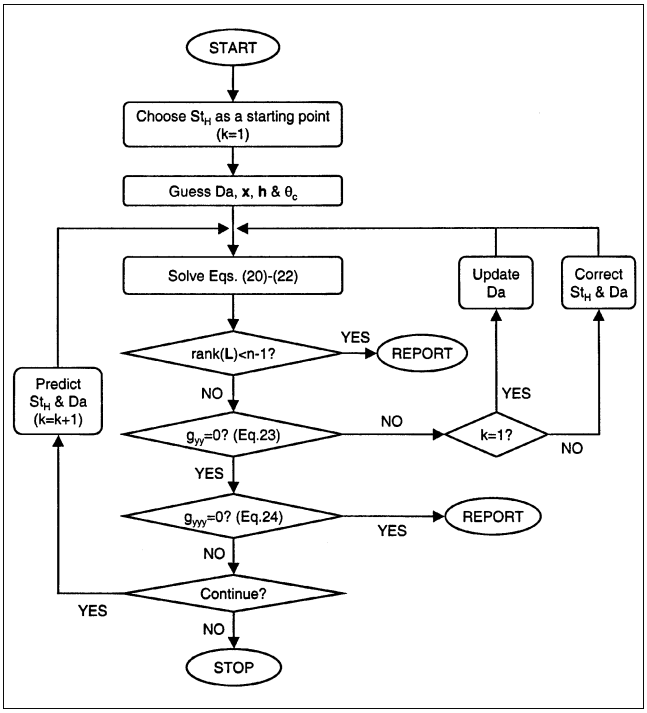

Figure 4. Calculation procedure of hysteresis locus on the (Da-St_H) plane.

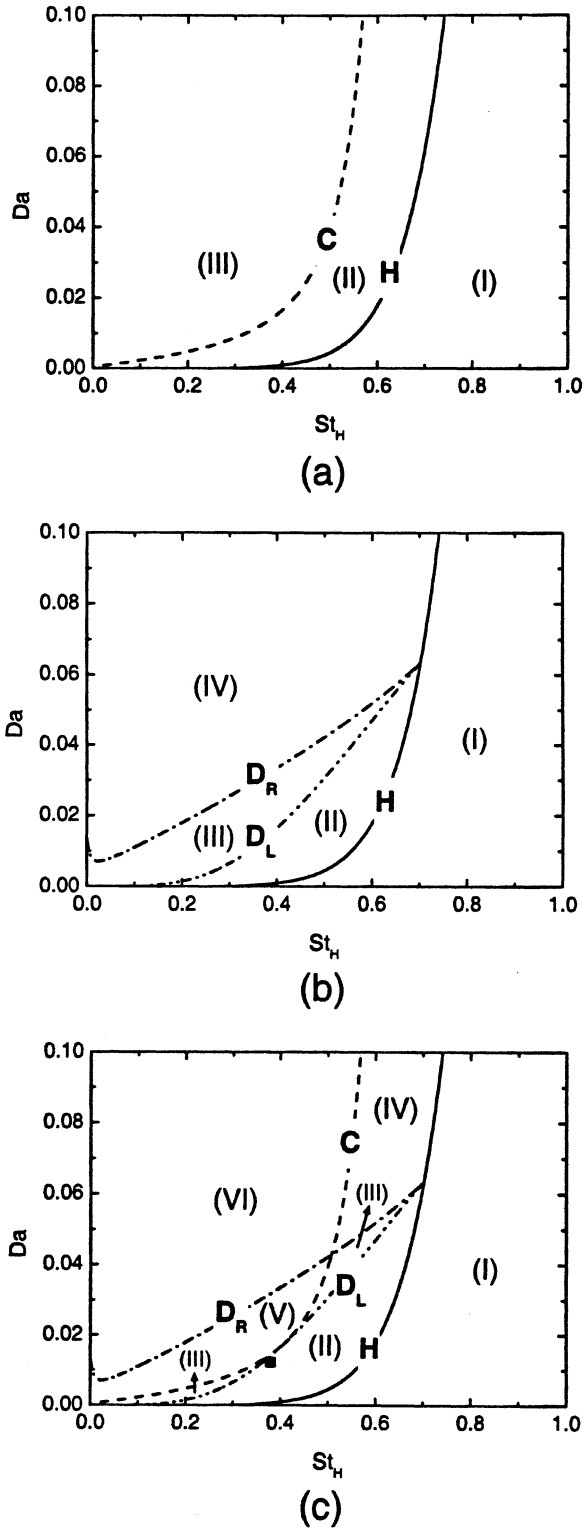

Figure 5. Critical boundaries on the (Da-St_H) plane: (a) hysteresis locus and control-limit boundary; (b) hysteresis locus and disjoint loci; and (c) overall multiplicity portrait.

quest is in regard to the left turning point, because of its association with a return to the original steady state, it would nevertheless be appropriate to investigate both turning points

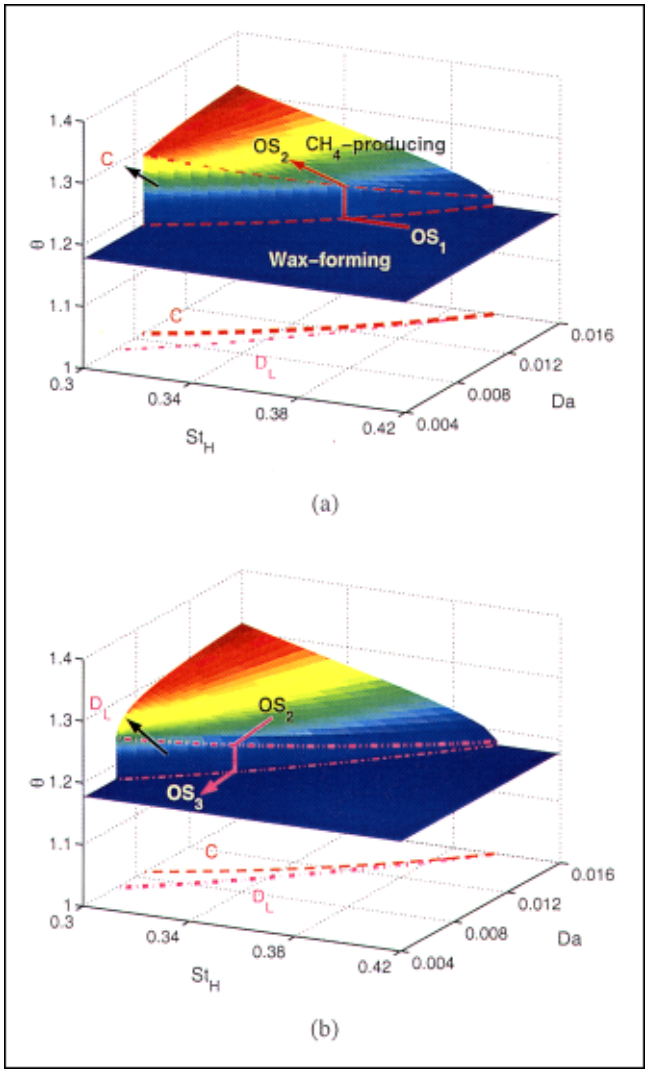

Figure 6. 3-D plot for explaining the steady-state jumping and the eventual recovery of the normal operating state.

for a more comprehensive analysis of the system's nonlinear behavior. These two boundaries (one for the left turning point denoted D_L and the other for the right, D_R) are called *disjoint loci* (Figure 5b). This terminology comes from the observation that the temperature curve becomes disjointed when it passes through these boundaries (for example, Russo and Bequette, 1995).

Four different regimes are distinguished in Figure 5b, each of which is associated with qualitatively distinct behavior. Suppose the process is moving from regime (II) to regime (III). Such a move is envisaged in the slow change of some process parameter relative to the time scale in which the reactor attains steady-state operation. In either of regimes II and III, the temperature curve is S-shaped, but on entering regime III the temperature curve is stripped off at the left turning point, as it is in the region forbidden by the constraint on the coolant temperature. If the process shifts further from regime III to regime IV, the lower branch of the temperature curve disappears into the forbidden region, leaving only the upper branch in the feasible region. In this case,

we will clearly have only the high-temperature steady state as the unique solution. Interestingly, these two disjoint curves meet at one point on the hysteresis locus. This occurs exactly where the left and the right turning points coalesce (at $\theta_c = 1$) to become the hysteresis point.

The control-limit boundary curve C meets the disjoint curve D_L tangentially and intersects the curve D_R transversally. Six different regimes are classified by the four different bifurcation boundaries, that is, hysteresis curve, control-limit boundary, and the two disjoint loci. While the nature of the different steady states is as described in prior figures (Figures 5a and 5b), a further subclassification is introduced by the disjoint loci. Indeed, the global multiplicity portrait in Figure 5c has a wealth of information about the process concerning the multiplicity features of the FT process and their variation in parameter space (specifically, the St_H–Da plane).

The initial operating state is marked by a square in Figure 5c (that is, $St_H = 0.38$ and $Da = 0.01225$, as shown in Table 1). The nominal operating conditions of Table 1 have been determined based on the reactor geometry and the operating conditions of our FT facility, at which the multiplicity was observed. The initial operating state is shown to locate quite close to the control-limit boundary C and the disjoint boundary D_L, which indicates that the initial operation of the FT process is not at a safe mode. If the system were to drift away from the neighborhood of this state, it runs the risk of an unfavorable switch in steady state, as is in fact suggested by the experimental observation that motivated the present investigation. Figure 6 provides a three-dimensional (3-D) close-up view of the neighborhood around the initial operating state (OS_1) of our process. Figure 6a shows how the steady state is forced to jump from the normal wax-forming mode (such as OS_1) to the undesirable methane-producing mode (such as OS_2), while Figure 6b accounts for the eventual recovery of the normal operating state (viz., from OS_2 to OS_3). The variable θ on the z-axis denotes the possible operating reaction temperature at the given (St_H, Da) coordinates. For example, if the process is operated on the blue planar surface parallel to the (St_H–Da) plane, it means that we can maintain the normal wax-producing mode by keeping the reaction temperature at the set point. However, in the course of reactor operation, one expects the heat-transfer coefficient and the catalyst activity to diminish somewhat, thus lowering both the dimensionless parameters St_H and Da. Thus, one may image a "drift" of the operating state in a direction below and to the left of its original position. If initially, the St_H decreases at a rate much faster than the activity of the catalyst, then the operating state OS_1 will move along the constant-Da line and eventually crosses the control-limit boundary C when it suddenly jumps to the higher reaction temperature. The control-limit boundary was shown as the vertical curvilinear wall in Figure 6a. The reaction temperature becomes higher as St_H continues its decrease, finally arriving at the new operating state (OS_2). The trajectory of the operating condition drifting with the decrease of St_H is represented as the red arrow in Figure 6a. This runaway scenario can also be understood by referring to Figure 3a, demonstrating clearly the jump in the operating temperature. The resulting high-temperature environment accelerates the catalyst deactivation, pushing the process to shift from OS_2 to some operating state OS_3. When the process transgresses the disjoint boundary D_L (that is, the vertical surface in Figure 6b), the previous steady state (or more precisely the normal operating state branch) will be recovered. The pink arrow from OS_2 to OS_3 indicates the operating temperature trajectory with the decrease of Da. The recovery of the normal operating temperature can also be well understood in Figure 3b. The recovered steady state (OS_3) is different from the initial steady state (OS_1), because the St_H and Da associated with OS_3 are, in fact, lower than those associated with OS_1; alternatively, the cooling capacity and heat-generation rate have both diminished for the new steady state at OS_3 below those at OS_1. We have thus a very plausible explanation of the experimentally observed phenomenon of an initial switch to a high-temperature steady state followed by a subsequent drop to the previous operation, albeit a lowered conversion because of diminished catalyst activity. It, therefore, appears that the envisaged variation in St_H and Da is consistent with the foregoing observations.

Finally, it is of interest to find an explanation of why the observations made have been sporadic. The pathway from OS_1 to OS_3 can, of course, be multifarious, and it is difficult to say which factors will determine the actual nature of this drift trajectory. Since we are concerned in this discussion only with steady states, we are oblivious to the submerged role of operating histories that will introduce considerable variability in the drift dynamics of the two salient parameters, St_H and Da. Because of the fact that the decrease in the parameters just given have opposing effects on steady-state multiplicity, it should be clear that what dictates the nature of the steady-state variation with time is the relative rates at which the two principal parameters decrease.

Impact of Feedback Controllers

It needs to be recalled here that the FT reactor analysis hitherto made is based on a simplified model, assuming that the process is completely stabilized by controllers throughout the operation. This approach was effective for probing the complex behavior of the FT reactor over the parameter space of relatively smaller dimensionality. Now, we are in a position to scrutinize that postulate mentioned earlier by investigating the impact of feedback controllers on the nonlinear features of the FT process. It is not only for confirming the conclusions of the earlier sections, but also for providing a more comprehensive understanding of the nonlinear characteristics of FT processes under control. For this purpose, the foregoing model, consisting of Eqs. 12 to 15, is expanded to include the cooler equation here, that is

$$\delta q_C(\Omega_{C,0}\theta_{C,0} - \Omega_C\theta_C) + St_H(\theta - \theta_C) = 0 \qquad (30)$$

where δ denotes the volume ratio of the reactor to the cooler and the subscript C denotes the cooler. The coolant flow rate q_c is determined by the imposed feedback control law. For the case of the proportional controllers (P-controllers), q_c is given by the following control law

$$q_C(\tau) = \bar{q}_C + \tilde{K}_c(\theta_{\mathrm{SET}} - \theta(\tau)) \qquad (31)$$

where $\tilde{K}_c$ is the control gain of P-controller, and θ_{SET} denotes the set temperature. The definitions of the newly intro-

duced dimensionless parameters in Eqs. 30 and 31 are shown below, and their nominal values are also given in Table 1

$$\Omega_{C,0} = \frac{\rho_{C,0} C_{pC,0}}{\rho_L C_{pL}}, \qquad \Omega_C = \frac{\rho_C C_{pC}}{\rho_L C_{pL}}$$
$$\delta = \frac{V}{V_C}, \qquad \tilde{K}_C = \frac{K_C}{Q_{G,0}/T_{C,0}} \tag{32}$$

For the sake of convenience, we call the models without and with the cooler equation the *ten-state* and *eleven-state* model, respectively, in the same way that Russo and Bequette (1995) did. In the *ten-state* model, the coolant temperature θ_c is directly regarded as the manipulated variable to control the reaction temperature, and it is also treated as the bifurcation parameter to search bifurcation points in nonlinear analysis. In the *eleven-state* model, on the other hand, the coolant flow rate, q_c, is employed as the manipulated variable and also as the bifurcation parameter, while θ_c subsequently becomes a state variable, which is a more realistic situation.

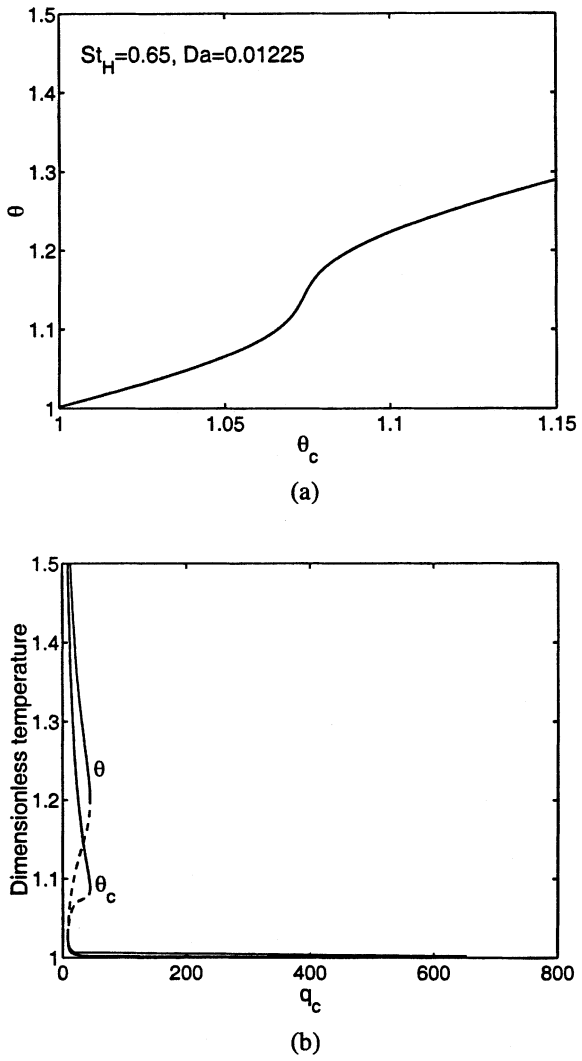

Figure 7. Sigmoidal temperature curves calculated by the ten-state and the eleven-state models.

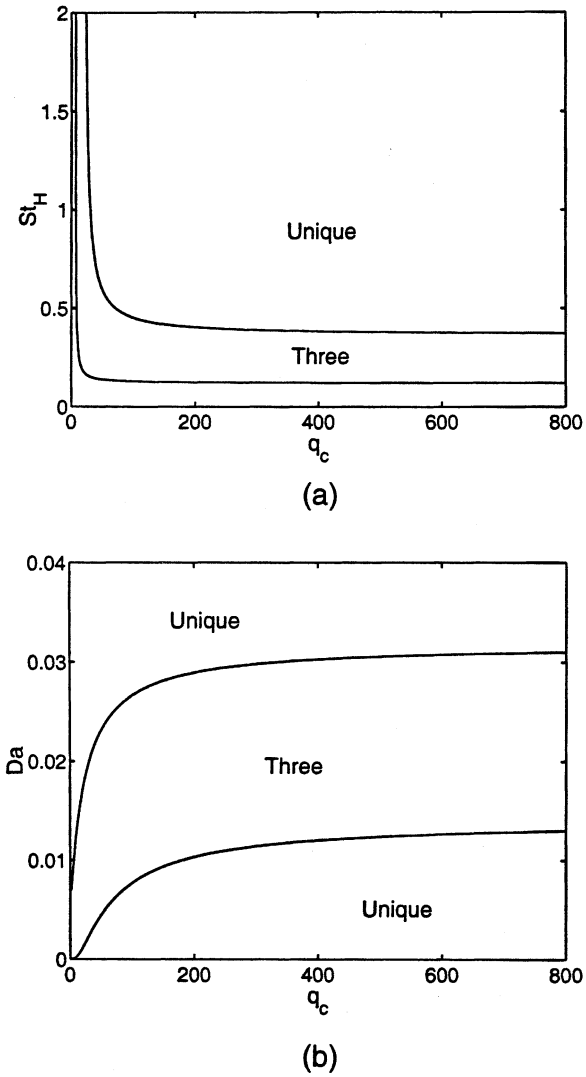

Figure 8. Multiplicity regions of the eleven-state model on (a) the (St_H-q_c), and (b) the (Da-q_c) planes.

Differences between ten- and eleven-state models

Figure 7 provides an example showing the difference of two models in multiplicity characteristics. At high St_H (that is, $St_H = 0.65$), the ten-state model exhibits only a unique solution (Figure 7a), whereas multiple steady states exist in the eleven-state model (Figure 7b). The resulting multiplicity region of the eleven-state model (Figure 8) is also different from that of the ten-state model (Figures 2b and 2d). This difference in multiplicity characteristics, brought out by the inclusion of the cooler equation, was reported for a general exothermic continuous stirred-rank reactor (CSTR) (Russo and Bequette, 1995).

Stability

In the ten-state model analysis made in the former sections, the loss of stability due to the controller failure was

ruled out among possible causes responsible for the observed steady-state shift. In order to verify the preceding postulate, it seems important to assure the existence of finite values for the control parameters capable of safely keeping the process stable during operation. More specifically, it is determined here that the controller gain, $\tilde{K}_C$, of the P-controller for stabilizing the process is within the reasonable range for physical implementation. If it is shown that the process is stabilized even by P-controllers, we can say that the stability would be much more easily achieved when PI- or PID-controllers are employed.

Figure 9 shows the stability change depending on $\tilde{K}_C$ at the nominal operating conditions (such as $St_H = 0.38$ and $Da = 0.01225$). The stable (solid line) and unstable (dashed line) operating states with no control actions are shown in Figure 9a. In order to stabilize the nominal operating state (that is, $\theta = 1.1772$), the magnitude of $\tilde{K}_C$ should be set sufficiently large. For example, even when $\tilde{K}_C = -5{,}000$ (Figure 9b), the operating state is still unstable, although the unstable region becomes smaller compared to the open-loop case. A much larger magnitude of $\tilde{K}_C$ (such as, $\tilde{K}_C = -15{,}000$) is required for the whole temperature branch to be stabilized (Figure 9c).

Interestingly, the process stability is affected not only by the control parameter settings but also by the process parameters. Figure 10 shows how the stability is affected by the variations of St_H and Da when $\tilde{K}_C$ is fixed as $-5{,}000$, as an example. The thicker lines in Figures 10a and 10b stand for the temperature profile at the nominal conditions. The decrease (increase) of St_H has a destabilizing (stabilizing) effect on the process stability (Figure 10a), while the decrease (increase) of Da has a stabilizing (destabilizing) effect (Figure 10b). As explained earlier, both of St_H and Da will be decreasing as the reaction proceeds, due to various reasons as conjectured previously. Thus, the stability may be hurt or enhanced, depending on the competitive effects of these two parameters decreasing with time. In either case, the choice of controllers as well as controller tuning should be carefully made considering the dependence of the stability on the process parameters under variation. The critical controller gain, $\tilde{K}_C^*$, will also be dependent on the process parameters. As shown in Figure 10c, the small magnitude of $\tilde{K}_C$ is enough to stabilize the operating state when St_H is relatively large. However, as St_H decreases, the magnitude of $\tilde{K}_C$ should exponentially increase for keeping the stable operation. Consequently the magnitude of $\tilde{K}_C^*$ goes to infinity as St_H asymptotically approaches a certain limiting value St_H^s. It means that if St_H becomes less than St_H^s, the nominal operating state cannot be stabilized by the P-controller. The effect of Da variation on the stability is exactly opposite to the effect of St_H variation, as shown in Figure 13 to be discussed subsequently. Thus, the magnitude of $\tilde{K}_C^*$ becomes large (small) as Da increases (decreases) and, if Da exceeds Da^s, there does not exist a $\tilde{K}_C$ capable of stabilizing the operating state (Figure 10d).

The preceding results suggest that we might not be able to justify our stability assumption for the case that St_H is seriously decreasing to be below St_H^s. Even though such a worst case is not encountered, it is still doubtful that the observed multiplicity behavior is indeed due to the limit of the control action, not to the controller failure. These questions will be clear in the next section.

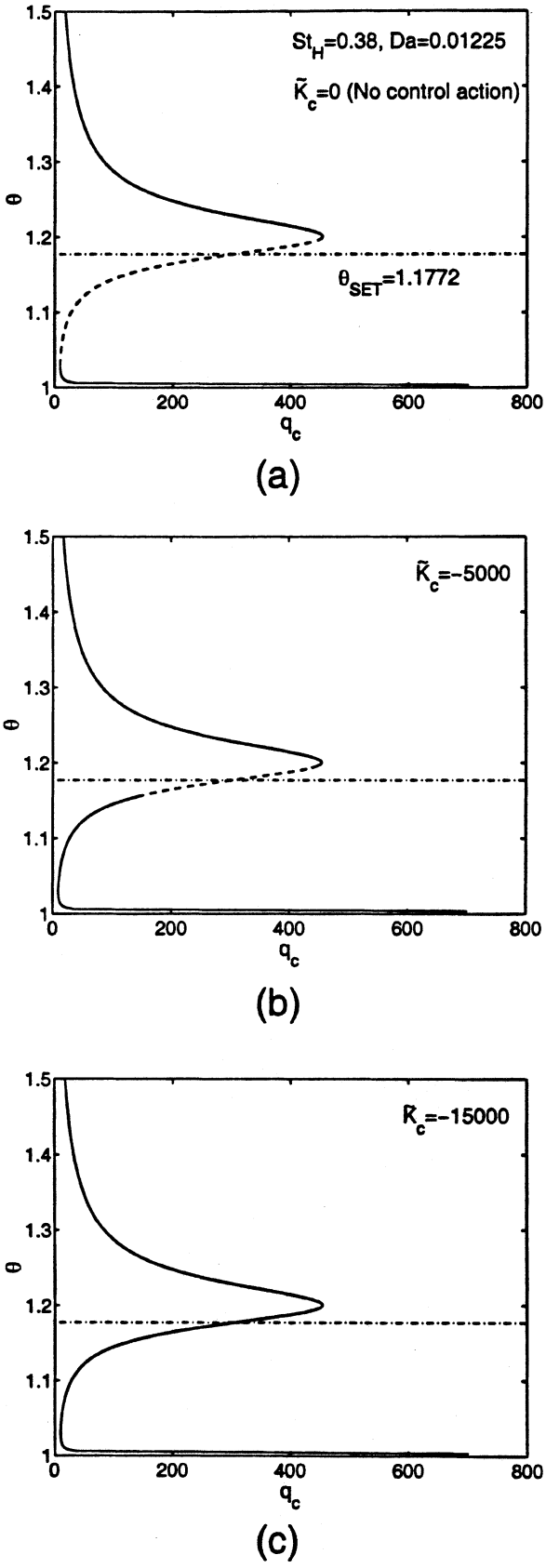

Figure 9. Stability change of temperature curve with various $\tilde{K}_C$: (a) $\tilde{K}_C = 0$, (b) $\tilde{K}_C = -5{,}000$, (c) $\tilde{K}_C = -15{,}000$.

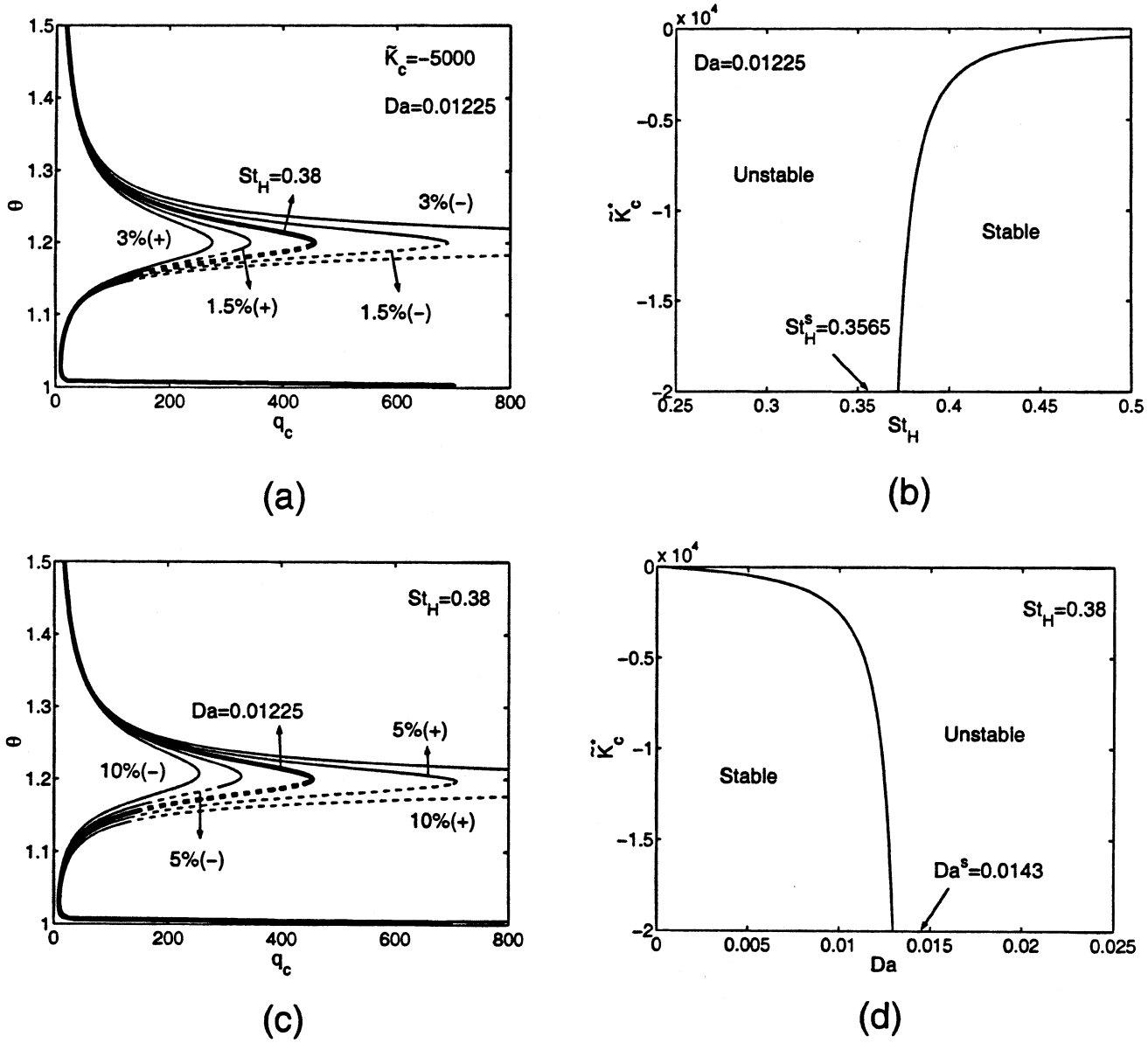

Figure 10. Effect of St_H and Da on the stability of temperature curves when $\tilde{K}_C = -5{,}000$ [(a) and (b)] and critical controller gain $\tilde{K}_C^*$ [(c) and (d)].

Reactor behavior

As described in detail earlier, the sudden jumping and the eventual returning between the two operating states, that is, wax- and methane-producing modes could be ascribed to the limit of the control action with the decrease of St_H and Da during operation, respectively. A more complete interpretation of the experimental observation can be provided here based on the new model, including the cooler equation where q_c is the manipulated variable instead of θ_c. Figure 11a explains how the normal wax-producing mode is suddenly switched over the methane-forming mode. $\tilde{K}_C$ is assumed to be set -10^6 (or equivalently $K_C = -0.0206$ m^3/°C in dimensional form), which is considered a sufficiently large but reasonable value for the implementation by controllers. OS_1 indicates the initial operating state. As St_H decreases (that is, as the heat-transfer coefficient becomes lower), a higher q_c is required to maintain the reaction temperature at the set-point. Thus, the operating state moves to the right as St_H decreases until q_c reaches its allowable maximum value, $q_{c,\max}$. For example, we suppose here the dimensionless maximum flow rate $q_{c,\max} = 2{,}000$ (or $Q_{c,\max} = 0.0175$ m^3/s in dimensional form), at which $\theta_c = 1.001$. Considering the fact that the realizable lowest value of the dimensionless coolant temperature is unity, we can also regard $q_{c,\max} = 2{,}000$ as a reasonable choice. OS_3 is the critical state when q_c is bound to $q_{c,\max}$. If even the slightest perturbation is introduced into this state, OS_3 would abruptly jump to higher temperature steady-state OS_4, where the product is switched from liquid hydrocarbons to undesirable methane gas. As St_H decreases further, the operating temperature becomes higher (OS_5).

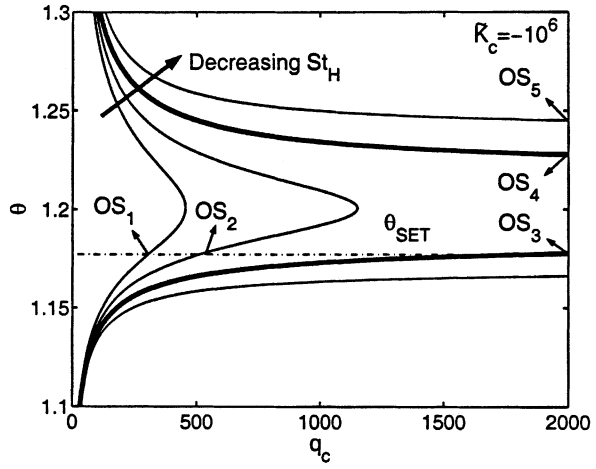

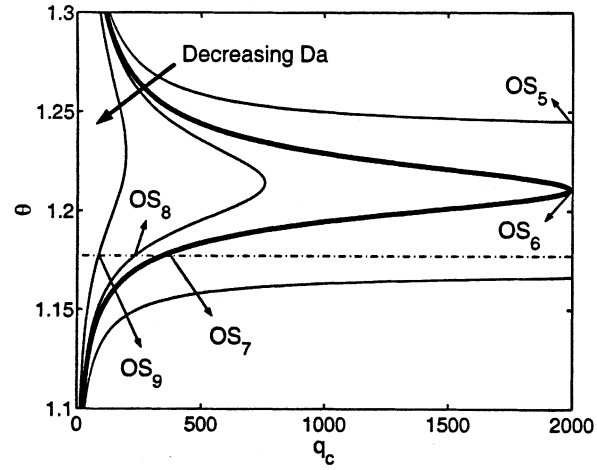

Figure 11. Effect of (a) St_H and (b) Da on sigmoidal temperature curves when $K_C = -10^6$ on the (θ-q_c) plane.

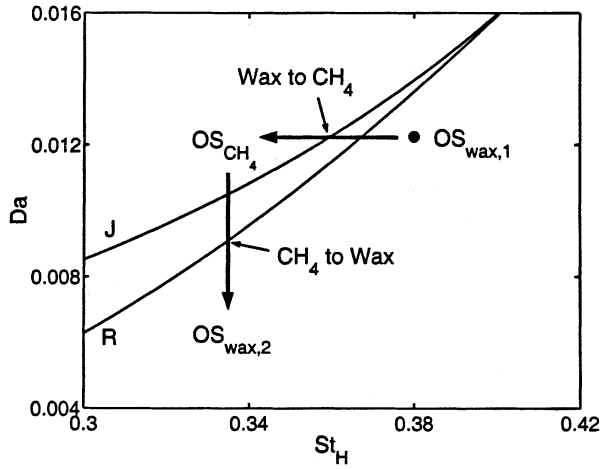

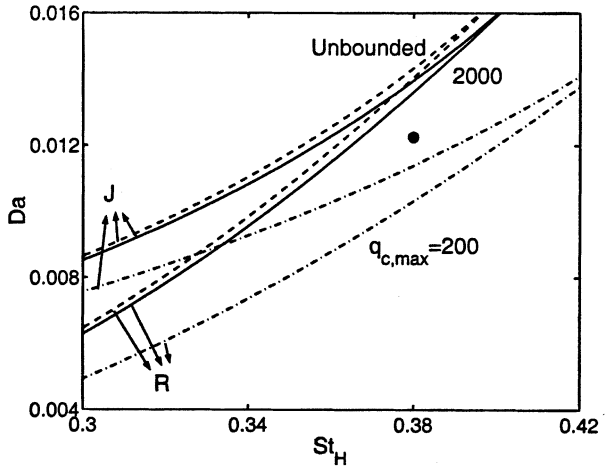

Figure 12. Critical boundaries for the steady-state jumping and the returning on the (Da-St_H) plane.

The return to the original normal operating state can be explained, based on similar reasoning. As Da decreases, the temperature curves shift to the left, as shown in Figure 11b and the operating state OS_5 will gradually move to the lower temperature state and arrive at OS_6, which is the critical situation for the recovery of the normal operating state. Then, the operating state is again switched from OS_6 to OS_7, where the hydrocarbons are again produced as the main product. The preceding scenario for explaining about the steady-state shift is basically the same as the one suggested in our previous study, except that q_c replace θ_c as the manipulated variable. However, the point to be noted here is that we have shown that the whole temperature curves can be kept stable against the decreasing St_H using only a simple P-controller with a reasonable value for the controller gain.

The critical boundaries for the jumping and the returning between those two distinguished steady states can be drawn on the ($Da-St_H$) plane (Figure 12a), providing a prospective view on the reactor behavior. $OS_{wax,1}$ indicates the initial operating state, where wax is being produced as the product. Since St_H and Da will be diminished in the course of reactor operation, we can expect that $OS_{wax,1}$ will eventually be moving to $OS_{wax,2}$. As assumed in Figure 11, if the St_H initially decreases as a rate much faster than the activity of the catalyst, then the operating state $OS_{wax,1}$ will move along the constant-Da line toward OS_{CH_4}. When it crosses the control-limit boundary, J (which was denoted as C in the earlier analysis of the ten-state model), $OS_{wax,1}$ suddenly jumps to the higher reaction temperature, producing mostly methane gas rather than wax. The resulting high-temperature environment accelerates the catalyst deactivation, pushing the process to shift from OS_{CH_4} to some other operating state, such as $OS_{wax,2}$. When the process transgresses the disjoint boundary R (which was denoted as D_L in the earlier analysis of the ten-state model), the previous normal wax-producing mode will be recovered. The recovered steady state ($OS_{wax,2}$) is different from the initial steady state ($OS_{wax,1}$), because the St_H and Da associated with $OS_{wax,2}$ are lower than those associated with

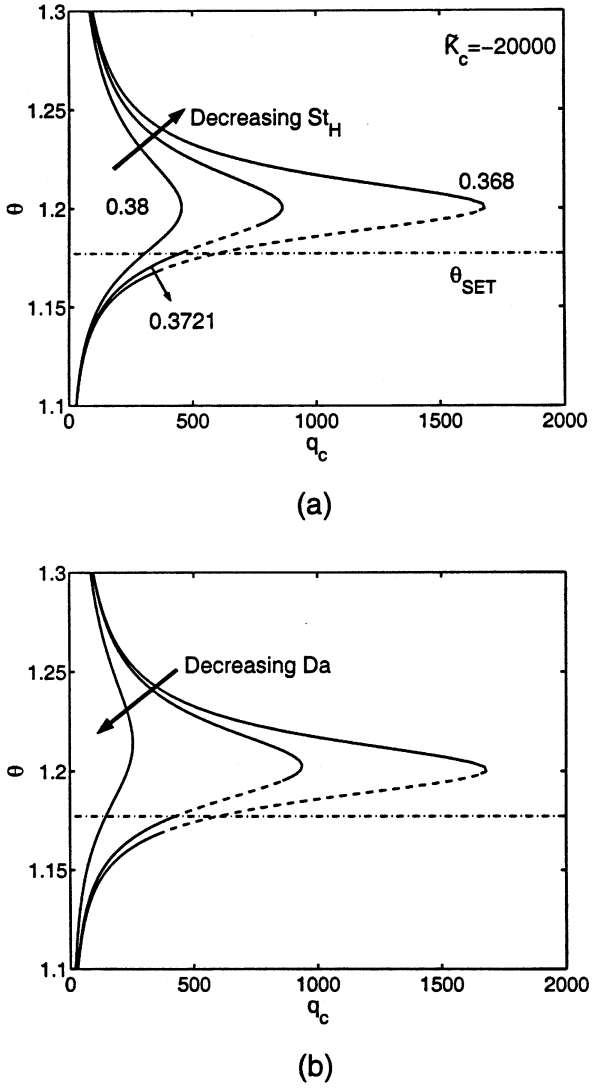

Figure 13. Effect of (a) St_H and (b) Da on sigmoidal temperature curves when $\tilde{K}_C = -20{,}000$ on the (θ-q_c) plane.

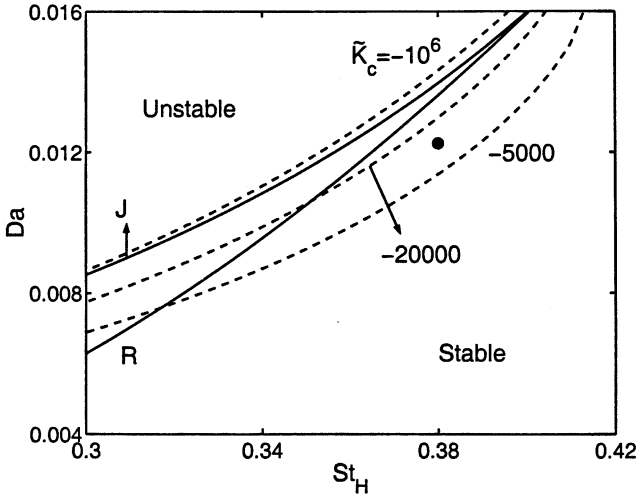

Figure 14. Critical boundaries for the loss of stability at the nominal operating states on the (Da-St_H) plane with various $\tilde{K}_C$.

$OS_{wax,1}$. This multiplicity phenomenon can be sporadic, since the pathway from $OS_{wax,1}$ to $OS_{wax,2}$ will vary depending on various factors such as initial condition, startup, and operation history. The boundaries J and R are of course functions of $q_{c,max}$. As $q_{c,max}$ becomes lower (larger), those boundaries will move such that the steady-state transitions take place at lower (higher) St_H and Da, as shown in Figure 12b.

Now, we consider the case when the controller gain is not sufficiently large. Although the results hitherto strongly support the proposition that the limit of the control variable is responsible for the observed multiplicity phenomenon, it is not clear at this stage whether the experimental observation also could be explained by the problem related to possible controller failure. Figure 13 can give an answer to this question. Suppose $\tilde{K}_C$ is set to be $-20{,}000$ (that is, $K_C = 4.1298 \times 10^{-4}$ m^3/°C in dimensional form). This value of $\tilde{K}_C$ might seem to be proper in the sense that the nominal operating state is stabilized at an initial stage. However, this choice of control parameters proves to be inappropriate when St_H becomes smaller with time. As shown in Figure 13a, the nominal operating state will eventually be unstable due to the stabilizing effect of the decreasing St_H. The reaction temperature cannot be maintained any more at the setpoint to irregularly move upward or downward toward the stable states, which will continue until the stability of the nominal operating state is recovered with the decrease of Da, as shown in Figure 13b. However, this undesirable behavior is not in tune with the experimental observation, vindicating again the conclusion of our previous study.

For achieving the safe operation of FT synthesis process, it is necessary to have an accurate understanding of the reactor behavior in regard to multiplicity as well as stability. It appears from the foregoing analysis that the jumping and the returning between the steady states occur due to the limit of the control action, rather than to the improper tuning of the controllers. Some critical boundaries practically important in FT reactors are drawn in the (St_H–Da) plane in Figure 14. Two solid curves denote the jump and the return between the steady states, and three dashed curves indicate the loss of the stability of the nominal operating state, depending on $\tilde{K}_C$. If the controller gain is set sufficiently large (such as, $\tilde{K}_C = -10^6$), it is the multiplicity problem that will be encountered during operation with the parameters variation. However, if $\tilde{K}_C$ is not set properly, for example, $\tilde{K}_C = -20{,}000$ or -5000, then the loss of stability would be the problem to be concerned about.

Conclusions

Complex multiplicity features in FT reactors have been systematically elucidated using singularity theory to interpret experimental observations of dynamic shifts in steady-state operation accompanied by significantly damaging variations in process performance. Local and global bifurcation analyses have helped provide a rational explanation of how an expected drop in cooling capacity and catalyst activity (reflected

in the decrease of the parameters St_H and Da with time) could be the plausible causes for the observed multiplicity behaviors in our FT system. Variations of these two parameters have opposite effects on the multiplicity. The decrease of St_H may cause the initial steady state (that is, nominal wax-producing mode) to be switched over to the high-temperature state (that is, undesirable methane-producing mode) by decreasing the cooling capacity of the cooler. The eventual recovery of the earlier steady state is attributed to the decrease of Da by deactivation of catalysts. From the global bifurcation diagram constructed based on the L-S reduction and the singularity theory, the sporadic nature of such steady-state transitions can be understood. The relative rates at which the parameters St_H and the Da decrease would determine the nature of the steady-state shifts observed in the FT reactor. This relative rate is clearly a function of transient effects associated with both startup and approach to steady states during shifts.

The preceding conclusions are corroborated as well when the dynamics of the cooler is considered in the bifurcation analysis of the process. Taking P-controller as an example, we could show that the observed multiplicity behavior is indeed not due to the loss of stability by poor tuning. It is also revealed that the process stability is impaired as St_H decreases but enforced as Da decreases, but there exists a reasonable range of the controller gain capable of stabilizing the process in spite of the deleterious effect on stability of the decreasing St_H during operation. In order to guarantee the safe operation of FT reactors, therefore, the choice of the controllers and control parameter settings should be carefully made, considering the dependence of the stability on the process parameter variations during operation.

Acknowledgment

Sincere gratitude is expressed to Conoco Inc., which provided financial support for this research.

Notation

a_{cat} = catalyst activity
C_{Gj} = concentration of species j in gas phase
$C_{Gj,0}$ = inlet concentration of species j in gas phase
C_{Lj} = concentration of species j in slurry phase
C_{pG} = heat capacity of gas phase
$C_{pG,0}$ = heat capacity of gas at the inlet conditions
C_{pL} = heat capacity of slurry phase
K_C = controller gain
E = activation energy
$h_C a_C$ = overall heat transfer coefficient per unit volume
He_j = Henry's constant for species j
$(-\Delta H_R)$ = heat of reaction per unit mole of CO
k = reaction rate constant of Eq. 8
K = reaction constant of Eq. 8
$(k_L a)_j$ = mass-transfer coefficient per unit volume for species j
P = pressure of the system
Q_G = volumetric flow rate of the gas phase
$Q_{G,0}$ = inlet volumetric flow rate of the gas phase
R = chemical reaction rate defined by Eq. 8 or universal gas constant
T = reaction temperature
T_C = coolant temperature
$T_{C,0}$ = inlet coolant temperature
$T_{G,0}$ = inlet gas temperature
V = reactor volume
V_C = cooler volume
w = catalyst loading in slurry

Greek letters

ϵ_G = gas holdup ratio
ν_j = stoichiometric coefficient for species j
ρ_G = density of gas phase
$\rho_{G,0}$ = density of gas phase at the inlet conditions
ρ_L = density of slurry phase

Literature Cited

Balakotaiah, V., and D. Luss, "Analysis of the Multiplicity Patterns of a CSTR," *Chem. Eng. Commun.*, **13**, 111 (1981).
Balakotaiah, V., and D. Luss, "Multiplicity Features of Reacting Systems: Dependence of the Steady-States of a CSTR on the Residence Time," *Chem. Eng. Sci.*, **38**, 1709 (1983).
Balakotaiah, V., and D. Luss, "Global Analysis of the Multiplicity Features of Multi-Reaction Lumped-Parameter Systems," *Chem. Eng. Sci.*, **39**, 865 (1984).
Balakotaiah, V., D. Luss, and B. L. Keyfitz, "Steady State Multiplicity Analysis of Lumped-Parameter Systems Described by a Set of Algebraic Equations," *Chem. Eng. Commun.*, **36**, 121 (1985).
Bhattacharjee, S., J. W. Tierney, and Y. T. Shah, "Thermal Behavior of a Slurry Reactor: Application to Synthesis Gas Conversion," *Ind. Eng. Chem. Process Des. Dev.*, **25**, 117 (1986).
Bukur, D. B., and R. F. Brown, "Fischer-Tropsch Synthesis in a Stirred Tank Slurry Reactor—Reaction Rates," *Can. J. Chem. Eng.*, **65**, 604 (1987).
Bukur, D. B., L. Nowicki, and X. Lang, "Fischer-Tropsch Synthesis in a Stirred Tank Slurry Reactor," *Chem. Eng. Sci.*, **49**, 4615 (1994).
Farr, W. W., and R. Aris, "Yet Who Would Have Thought the Old Man to Have Had so Much Blood in Him?—Reflections on the Multiplicity of Steady States of the Stirred Tank Reactor," *Chem. Eng. Sci.*, **41**, 1385 (1986).
Gilmore, R., *Catastrophe Theory for Scientists and Engineers*, Dover, New York (1981).
Golubitsky, M., and B. L. Keyfitz, "A Qualitative Study of the Steady-State Solutions for a Continuous Flow Stirred Tank Chemical Reactor," *SIAM J. Math Anal.*, **11**, 316 (1980).
Golubitsky, M., and D. G. Schaeffer, "A Theory for Imperfect Bifurcation via Singularity Theory," *Commun. Pure Appl. Math.*, **32**, 21 (1979).
Golubitsky, M., and D. G. Schaeffer, *Singularities and Groups in Bifurcation Theory*, Vol. I, Springer-Verlag, New York (1985).
Gormley, R. J., M. F. Zarochak, P. W. Deffenbaugh, and K. R. P. M. Rao, "Effect of Initial Wax Medium on the Fischer-Tropsch Slurry Reaction," *Appl. Catal. A*, **161**, 263 (1997).
Hilmen, A. M., D. Schanke, K. F. Hanssen, and A. Holmen, "Study of the Effect of Water on Alumina Supported Cobalt Fischer-Tropsch Catalysts," *Appl. Catal. A*, **186**, 169 (1999).
Kirillov, V. A., V. M. Khanaev, V. D. Meshcheryakov, S. I. Fadeev, and R. G. Luk'yanova, "Numerical Analysis of Fischer-Tropsch Processes in Reactors with a Slurried Catalyst Bed," *Theor. Found. Chem. Eng.*, **33**, 270 (1999).
Liu, Z.-T., Y.-W. Li, J.-L. Zhou, Z.-X. Zhang, and B.-J. Zhang, "Deactivation Model of Fischer-Tropsch Synthesis over an Fe-Cu-K Commercial Catalyst," *Appl. Catal. A*, **161**, 137 (1997).
Lox, E. S., and G. F. Froment, "Kinetics of the Fischer-Tropsch Reaction on a Precipitated Promoted Iron Catalyst. 1. Experimental Procedure and Results," *Ind. Eng. Chem. Res.*, **32**, 61 (1993a).
Lox, E. S., and G. F. Froment, "Kinetics of the Fischer-Tropsch Reaction on a Precipitated Promoted Iron Catalyst. 2. Kinetic Model," *Ind. Eng. Chem. Res.*, **32**, 71 (1993b).
Maretto, C., and R. Krishna, "Modelling of a Bubble Column Slurry Reactor for Fischer-Tropsch Synthesis," *Catal. Today*, **52**, 279 (1999).
Russo, L. P., and B. W. Bequette, "Impact of Process Design on the Multiplicity Behavior of a Jacketed Exothermic CSTR," *AIChE J.*, **41**, 135 (1995).
Satterfield, C. N., and G. A. Huff, Jr., "Mass Transfer and Product Selectivity in a Mechanically Stirred Fischer-Tropsch Slurry Reactor," *ACS Symp.*, **196**, 225 (1982).

Seydel, R., *Practical Bifurcation and Stability Analysis*: *From Equilibrium To Chaos*, Springer-Verlag, New York (1994).
Shah, Y. T., C. G. Dassori, and J. W. Tierney, "Multiple Steady States in Non-Isothermal FT Slurry Reactor," *Chem. Eng. Commun.*, **88**, 49 (1990).
Song, H.-S., D. Ramkrishna, S. Trinh, R. L. Espinoza, and H. Wright, "Multiplicity and Sensitivity Analysis of Fischer-Tropsch Bubble Column Slurry Reactors: Plug-Flow Gas and Well-Mixed Slurry Model," *Chem. Eng. Sci.*, **58**, (12), 2759 (2003).
Stern, D., A. T. Bell, and H. Heinemann, "A Theoretical Model for the Performance of Bubble-Column Reactors Used for Fischer-Tropsch Synthesis," *Chem. Eng. Sci.*, **40**, 1665 (1985).
Van Der Laan, G. P., and A. A. C. M. Beenackers, "Kinetics and Selectivity of the Fischer-Tropsch Synthesis: A Literature Review," *Catal. Rev.— Sci. Eng.*, **41**, 255 (1999).
Withers, H. P., K. F. Eliezer, and J. W. Mitchell, "Slurry-Phase Fischer-Tropsch Synthesis and Kinetic Studies over Supported Cobalt Carbonyl Derived Catalysts," *Ind. Eng. Chem. Res.*, **29**, 1807 (1990).
Yermakova, A., and V. I. Anikeev, "Thermodynamic Calculations in the Modeling of Multiphase Processes and Reactors," *Ind. Eng. Chem. Res.*, **39**, 1453 (2000).

Manuscript received June 19, 2002, revision received Jan. 23, 2003, and final revision received Mar. 17, 2003.